

Inducing localized solutions via interaction in a self-defocusing system with localized pumping

Wesley B. Cardoso¹ and Mateus C. P. dos Santos²

¹*Instituto de Física, Universidade Federal de Goiás, 74.690-900, Goiânia, Goiás, Brazil*

²*Instituto de Ciências Tecnológicas e Exatas, Universidade Federal do Triângulo Mineiro, 38064-200, Uberaba, Minas Gerais, Brazil*

We investigate the emergence of induced localized coupled modes in passive cavities with both loss and gain. Our model is based on linearly coupled Lugiato-Lefever equations, where a Gaussian pump beam is applied to only one mode. Through numerical simulations, we demonstrate that self-defocusing systems can support the formation of localized stationary modes in the partner field. The characteristics of these induced modes are determined by key parameters, including coupling strength, cavity decay rate, detuning effects, and the pump beam's intensity and width.

I. INTRODUCTION

Solitons are a significant class of solutions emerging from nonlinear wave equations, characterized by a precise equilibrium between dispersive and nonlinear effects. These self-sustained waveforms preserve their shape as they propagate and exhibit distinct nonlinear interactions during collisions [1–3]. The prevalent presence of nonlinear wave equations in physics allows solitons to emerge across multiple fields, such as water waves [4–6], nonlinear fiber optics [3, 7, 8], plasmas [9–11], Bose-Einstein condensates (BECs) [12–14], and degenerate fermion mixtures [15]. Experimental observation has been the focus of extensive research, leading to its realization in various physical systems, including vapors of alkali metals [16] and nonlinear waveguides [17, 18].

In particular, there is a class of solitons that emerge from dissipative systems [19, 20], commonly found in nonlinear optics. Although these models typically lack integrability, they provide a more realistic description of various physical configurations. In dissipative media, optical profiles are sustained by external pumping in the form of laser beams. For passive optical systems, such solitons are described by the Lugiato-Lefever (LL) equation [21]. This equation has been widely used to model Kerr frequency combs [22–26], contributing to advancements in spectroscopy [27], optical metrology [28], radio-frequency photonics [29], and optical communications [30].

A natural extension of passive optical systems (spatial or temporal domain) with gain and loss is to consider an optical system where multiple electromagnetic modes interact with each other within a cavity in a dissipative nonlinear medium. With pumping applied to each mode, the localization and dynamics of the coupled solitons are described by the set of coupled LL equations [31–34]. In these configurations, the modes are self-sustained through the interplay of dispersion, diffraction, nonlinear effects, pumping, dissipation, and their mutual interactions. In this context, the coupling of electromagnetic modes in optical systems allows the study of vortex solitons [35], vector cavity solitons [36], formation of dark dissipative solitons [37], and the dy-

namics of high-order cavity solitons [38]. In Ref. [39] the authors investigate the role of coupling between clockwise and counterclockwise propagating modes in the generation of Kerr frequency combs within whispering-gallery microcavities. Both numerical and experimental analyses confirm that soliton formation and comb power distribution are strongly influenced by the coupling strength. The study employs coupled LL equations with a constant external pump applied to a single mode to demonstrate Kerr comb generation.

Recently, the inclusion of a localized pump has shown great potential for generating stable optical beams whose localization patterns directly reflect the pump profile [40–43]. Specifically, in Ref. [42], the authors introduce a model of a passive optical cavity based on a two-dimensional variant of the Lugiato-Lefever equations, incorporating a localized pump with intrinsic vorticity S and considering both cubic and cubic-quintic nonlinearities. On the other hand, the induction of localized solutions in partner fields – including cases exhibiting symmetry breaking – solely due to coupling has been investigated in [44–47]. However, previous studies on this phenomenon have been limited to systems governed by nonlinear Schrödinger equations in the absence of an external pump, leaving open the question of how a localized pump may influence the coupling dynamics and the formation of localized states in dissipative systems. In the present work, we examine the impact of linear coupling on the localization of interacting optical modes in a dissipative nonlinear cavity with spatially inhomogeneous pumping applied to only one mode. Unlike previous studies, our focus is on the induction of localized structures and the transfer of profile characteristics mediated by the coupling mechanism. Additionally, we investigate the influence of cavity decay rates and detuning, as well as the modifications induced by variations in the pump beam's spatial profile.

The remainder of this paper is structured as follows: the next section introduces the theoretical model; Sec. III presents the numerical results, detailing the characteristics and conditions for the induction of localization; finally, Sec. IV provides the concluding remarks.

II. THEORETICAL MODEL

Consider a system that describes the dynamics of two interacting fields in a localized pumping system, whose mathematical model is well described by coupled LL equations, which are often used to model optical cavities with dissipation and nonlinearity, given by:

$$\frac{\partial E_1}{\partial t} = \left[-(\alpha_1 + i\Delta_1) + i\frac{\partial^2}{\partial x^2} - i|E_1|^2 \right] E_1 + i\kappa E_2 + F(x), \quad (1)$$

$$\frac{\partial E_2}{\partial t} = \left[-(\alpha_2 + i\Delta_2) + i\frac{\partial^2}{\partial x^2} - i|E_2|^2 \right] E_2 + i\kappa E_1, \quad (2)$$

where $E_1(x, t)$ and $E_2(x, t)$ are complex fields, representing the intensity profile of the two fields in time and space; α_1 and α_2 are damping rates of each field; Δ_1 and Δ_2 are frequency shift (or phase adjustment) parameters of fields 1 and 2, respectively; $\partial^2/\partial x^2$ is the spatial diffusion term, representing the dispersion (or diffusion) of the field along the spatial coordinate x ; $|E_1|^2$ and $|E_2|^2$ are the contributions due to Kerr-type nonlinearities; κ represents the interaction between the fields E_1 and E_2 , allowing them to mutually influence their dynamics. $F(x)$ is the external pumping applied exclusively to the field E_1 .

Note that the nonlinearity of the system is self-defocusing for both fields, which means that there can be no equilibrium between the dispersion/diffusion and the nonlinear effects of the system (i.e., no localized solution) in the absence of pumping. In this study, we will investigate the influence of the pumping term on the localization of field 1 and how the interaction between the fields induces localization in the partner field.

As an example of localized pumping, in this work, we will employ a Gaussian pump described by the following expression:

$$F(x) = \frac{P_0}{\sqrt{\pi}W} \exp\left(-x^2/W^2\right), \quad (3)$$

where P_0 and W represent the pump intensity and width, respectively.

III. NUMERICAL RESULTS

In this section, we present the numerical results derived from Eqs. (1) and (2), with a localized pump applied to field E_1 as specified in Eq. (3). The numerical integration was performed using a pseudo-spectral method, where the diffusive term in x was addressed using the fast Fourier transform, and the temporal evolution was solved using the 4th-order Runge-Kutta method. We employed 256 spectral points over a

spatial domain of size 40, with a time step of 10^{-3} . The system was initialized with both fields in the vacuum state and evolved until convergence of the localized solution was achieved. For more details on this methodology, we direct the reader to the reference book [48].

Influence of coupling parameter κ : First, we will examine the influence of the coupling parameter on the localization of the partner field. To this end, Fig. 1 presents an example of the intensity profiles of the fields for three different values of this parameter, while keeping all other system parameters fixed. It can be observed that, as the coupling parameter increases, the partner field exhibits greater power, eventually surpassing the power of field E_1 . Indeed, we find that for the same values of the other parameters used in Fig. 1, the powers of both fields become equal when κ is approximately 2.0.

To further illustrate this, Fig. 2(a) shows the relationship between the powers of the fields and the coupling parameter κ . It is worth noting that the power values begin to decrease after a certain κ threshold. Moreover, the maximum power for field E_2 is reached when it equals the power of field E_1 . In another simulation, we observed that increasing the detuning shifts the peak of the power curve to higher values of κ . This result is illustrated in Fig. 2(b), where we set $\Delta_1 = \Delta_2 = 2$, while keeping the other parameter values the same as those used to produce Fig. 2(a). Note that the values of the two powers now become equal for $\kappa \simeq 2.9$. Next, in Fig. 2(c), a similar behavior can be observed, but now considering a higher decay rate, i.e., $\alpha_1 = \alpha_2 = 2$, while keeping the other parameter values the same as those used in Fig. 1. In this case, the power values coincide when $\kappa \simeq 2.8$.

Influence of decay rates $\alpha_{1,2}$: In order to investigate the influence of the decay parameter on the induction of localization in the partner field (E_2), we first analyze the behavior of the power for the symmetric case of this parameter, i.e., choosing equal values for the decay rates $\alpha_1 = \alpha_2 = \alpha$. The result of our simulation is shown in Fig. 3(a), where it can be observed that the higher the value of α , the lower the power of both fields. Moreover, the power of the induced field rapidly decreases to values close to zero, reaching $P_2 \simeq 0.004$ when $\alpha = 5$.

In the result shown in Fig. 3(b), we kept the decay rate of field E_2 fixed at $\alpha_2 = 1$, while varying the value of α_1 . We observed a similar behavior to that presented in Fig. 3(a), indicating that the decay rate of field E_1 significantly impacts the response of the induced field E_2 . On the other hand, to examine the impact of the decay rate of field E_1 , in Fig. 3(c) we kept it fixed at $\alpha_1 = 1$ while varying the value of α_2 . It can be seen that as α_2 increases, the power of field E_2 approaches zero, while the power of field E_1 stabilizes at a value close to 0.78. Therefore, when the ratio α_1/α_2 becomes very large, the induction effect is lost, causing field E_2 to vanish while maintaining the localized structure of field E_1 .

Frequency Detuning Effect Δ : In Fig. 4, we present

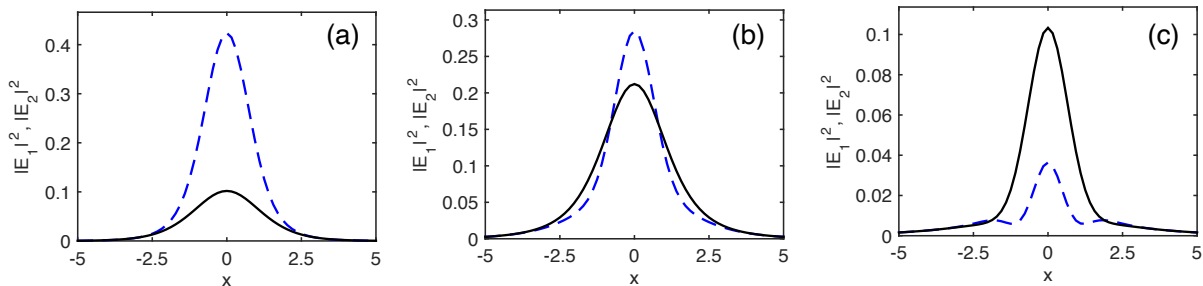


Figure 1. Numerical profile of the intensities ($|E_1|^2$ and $|E_2|^2$, represented by dashed and solid lines, respectively) of the localized states after their respective stabilization for three different values of the coupling parameter, specifically (a) $\kappa = 1$, (b) $\kappa = 2$, and (c) $\kappa = 5$. The system starts from the vacuum as the initial state. The other parameter values are $\Delta_1 = \Delta_2 = \alpha_1 = \alpha_2 = W = 1$ and $P_0 = 3$.

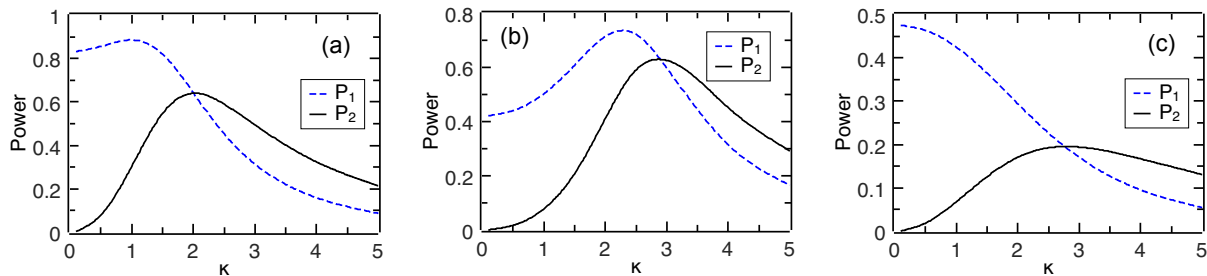


Figure 2. Power of the fields E_1 and E_2 as a function of κ . In panel (a), the parameter values are the same as those used in Fig. 1. In panel (b), we modify the values to $\Delta_1 = \Delta_2 = 2$ (keeping the other parameter values the same). In panel (c), we set $\alpha_1 = \alpha_2 = 2$ and keeping the other parameter values the same as in Fig. 1.

the analysis of the impact resulting from changes in the detuning. Specifically, in Fig. 4(a), we consider the symmetric case, where both fields have the same detuning ($\Delta_1 = \Delta_2 = \Delta$). We can observe that the power is higher when a redshift is applied (negative values of Δ). For field E_1 , two prominent power peaks occur at $\Delta \simeq -1.8$ and $\Delta \simeq 0.5$, with the former exhibiting a higher power. The induced field, on the other hand, exhibits a single power peak at $\Delta = -0.9$.

In Fig. 4(b), we analyze the influence of detuning solely for field E_1 , keeping $\Delta_2 = 1$ fixed. Interestingly, unlike the symmetric case shown in Fig. 4(a), the power of field E_1 now exhibits a single peak at $\Delta_1 \simeq -0.7$, while the power peak of E_2 occurs at $\Delta_1 \simeq -0.25$. Finally, in Fig. 4(c), we observe the behavior of the powers as a function of Δ_2 only, with $\Delta_1 = 1$. Here, we can see that Δ_2 introduces a significant change in the power of the induced solution, reaching a maximum at $\Delta_2 = -0.1$. Additionally, the power of field E_1 also undergoes more pronounced changes when Δ_2 is close to zero.

Influence of Pump Amplitude P_0 : We now analyze the changes in the induced solution when considering different values of the pump amplitude. In this regard, Fig. 5 shows how the power of solutions E_1 and E_2 varies with changes in this parameter. Specifically, in Fig. 5(a), we consider a positive detuning (blueshift), while in Fig.

5(b), we examine the opposite case. Note that the behavior of the powers is similar in that both increase as the pump amplitude rises. Moreover, when the detuning is negative (Fig. 5(b)), the induced field exhibits a larger power increase compared to the case with positive detuning (Fig. 5(a)), as previously observed in Fig. 4. However, the gap between the powers in the negative detuning case is smaller, as can be visually observed in Fig. 5.

Influence of Pump Width W : Our final study involves analyzing the dependence of the pump width on the induction of localization in the partner field E_2 . A summary of the numerical results is presented in Fig. 6, where the power of the solutions E_1 and E_2 is shown in Fig. 6(a), while the corresponding average width is displayed in Fig. 6(b). To calculate the average width, we used the definition

$$\langle x^2 \rangle = \int_{-\infty}^{\infty} x^2 |E_k|^2 dx,$$

where the index $k = 1$ or 2 corresponds to the calculation of the average width for field E_1 or E_2 , respectively. Furthermore, these figures illustrate the results of our simulations for two distinct detuning values, namely $\Delta_1 = \Delta_2 = 1$ and $\Delta_1 = \Delta_2 = -1$.

In Fig. 6(a), it can be observed that the power of the solutions decreases as the pump width increases. Ad-

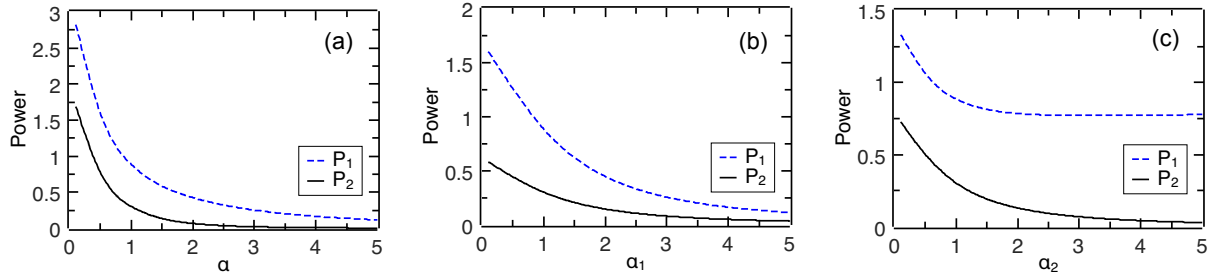


Figure 3. Power of the fields E_1 and E_2 as a function of decay rate. (a) Symmetric case, considering $\alpha_1 = \alpha_2 = \alpha$; (b) Field E_2 with a fixed decay rate $\alpha_2 = 1$; (c) Field E_1 with a fixed decay rate $\alpha_2 = 1$. The other parameter values were $\Delta_1 = \Delta_2 = \kappa = W = 1$ and $P_0 = 3$.

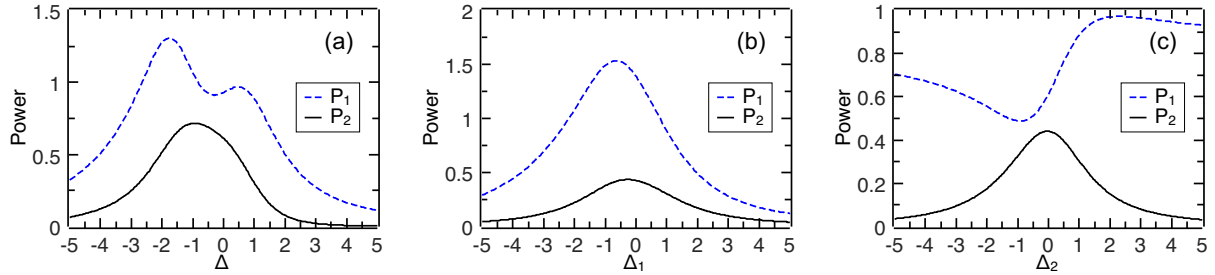


Figure 4. Power of the fields E_1 and E_2 as a function of the frequency shift. In panel (a), the symmetric case is presented, with $\Delta_1 = \Delta_2 = \Delta$. The variation of Δ_1 only is shown in panel (b), where we fix $\Delta_2 = 1$. In panel (c), we reverse the setup, fixing $\Delta_1 = 1$ while varying Δ_2 . The other parameter values were $\alpha_1 = \alpha_2 = \kappa = W = 1$ and $P_0 = 3$.

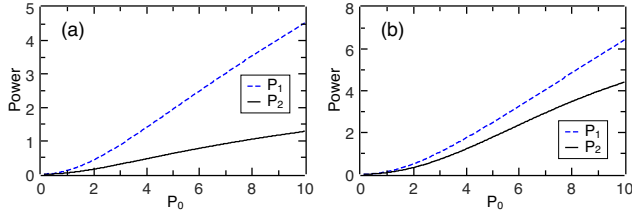


Figure 5. Power as a function of the pump intensity P_0 , considering (a) $\Delta_1 = \Delta_2 = 1$ and (b) $\Delta_1 = \Delta_2 = -1$. The other parameter values used here were $\alpha_1 = \alpha_2 = \kappa = W = 1$.

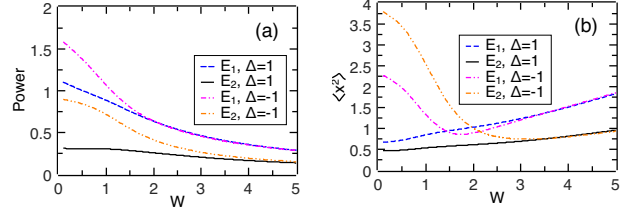


Figure 6. (a) Power and (b) average width of the solutions for fields E_1 and E_2 as a function of the pump width W , for two distinct values of detuning. The other parameter values used here were $\alpha_1 = \alpha_2 = \kappa = 1$ and $P_0 = 3$.

ditionally, it is noteworthy that as W increases, the difference between the power obtained for both detuning values diminishes, becoming indistinguishable beyond a certain value of W . This result is also observed when examining the average width shown in Fig. 6(b), where the values become indistinguishable at approximately $W > 3.5$, for both fields.

Another interesting result pertains to the relationship between power and average width for small values of W . Note that the power of field E_1 is always greater than that of field E_2 . However, for the negative detuning value, we observe that the width of field E_2 is larger than that of E_1 , which is the opposite of what occurs when the detuning is positive. Furthermore, when the detuning is negative, there is a point where the widths of both

solutions are equal, corresponding to $W \simeq 2.15$.

IV. CONCLUSION

In conclusion, we investigated the induction of localized solutions in a self-defocusing nonlinear optical system with localized pumping, emphasizing the role of linear coupling in shaping the formation of structured optical fields. Through numerical simulations, we analyzed the influence of key system parameters, including the coupling strength κ , decay rates α_1 , α_2 , frequency detuning Δ , pump amplitude P_0 , and pump width W . Our results demonstrate that the interaction between the coupled fields E_1 and E_2 plays a fundamental role

in defining the localization dynamics, with the induced stationary modes exhibiting distinct characteristics depending on the coupling strength and the spatial properties of the pump.

Notably, our findings reveal that, even in the absence of direct excitation, localized states can emerge in the partner field solely due to the coupling mechanism. This behavior is strongly influenced by the interplay between detuning and dissipation, which governs the stability and spatial distribution of the induced modes.

Our study extends previous investigations on coupled nonlinear optical systems by incorporating the effects of a spatially inhomogeneous pump, highlighting new possibilities for tailoring localized states through controlled interactions. These results contribute to the broader understanding of dissipative solitons and struc-

tured light in nonlinear cavities, with potential applications in photonic information processing and optical trapping.

ACKNOWLEDGMENTS

We acknowledge the financial support provided by the Brazilian agencies CNPq (grant #306105/2022-5 and Sisphoton Laboratory- MCTI No. 440225/2021-3), CAPES, and FAPEG. This work was also performed as part of the Brazilian National Institute of Science and Technology (INCT) for Quantum Information (Grant No. 465469/2014-0).

-
- [1] N. J. Zabusky and M. D. Kruskal, *Phys. Rev. Lett.* **15**, 240 (1965).
- [2] Y. S. Kivshar and B. A. Malomed, *Rev. Mod. Phys.* **61**, 763 (1989).
- [3] Y. S. Kivshar and G. P. Agrawal, *Optical solitons: from fibers to photonic crystals* (Academic press, 2003).
- [4] W. Craig, P. Guyenne, J. Hammack, D. Henderson, and C. Sulem, *Physics of Fluids* **18**, 057106 (2006).
- [5] Y. Kodama, *Journal of Physics A: Mathematical and Theoretical* **43**, 434004 (2010).
- [6] M. J. Ablowitz and D. E. Baldwin, *Phys. Rev. E* **86**, 036305 (2012).
- [7] A. Hasegawa and Y. Kodama, *Solitons in optical communications* (Oxford University Press, 1995).
- [8] M. Erkintalo, K. Hammani, B. Kibler, C. Finot, N. Akhmediev, J. M. Dudley, and G. Genty, *Phys. Rev. Lett.* **107**, 253901 (2011).
- [9] K. E. Lonngren, *Plasma Physics* **25**, 943 (1983).
- [10] L. Bergé, *Physics Reports* **303**, 259 (1998).
- [11] P. K. Shukla and A. A. Mamun, *New Journal of Physics* **5**, 17 (2003).
- [12] S. Burger, K. Bongs, S. Dettmer, W. Ertmer, K. Sengstock, A. Sanpera, G. V. Shlyapnikov, and M. Lewenstein, *Phys. Rev. Lett.* **83**, 5198 (1999).
- [13] K. E. Strecker, G. B. Partridge, A. G. Truscott, and R. G. Hulet, *Nature* **417**, 150 (2002).
- [14] L. Khaykovich, F. Schreck, G. Ferrari, T. Bourdel, J. Cubizolles, L. D. Carr, Y. Castin, and C. Salomon, *Science* **296**, 1290 (2002).
- [15] S. K. Adhikari, *The European Physical Journal D-Atomic, Molecular, Optical and Plasma Physics* **40**, 157 (2006).
- [16] J. E. Bjorkholm and A. A. Ashkin, *Phys. Rev. Lett.* **32**, 129 (1974).
- [17] J. W. Fleischer, M. Segev, N. K. Efremidis, and D. N. Christodoulides, *Nature* **422**, 147 (2003).
- [18] *Physics Reports* **463**, 1 (2008).
- [19] H. B. H.-G. Purwins and S. Amiranashvili, *Advances in Physics* **59**, 485 (2010).
- [20] P. Grelu and N. Akhmediev, *Nature photonics* **6**, 84 (2012).
- [21] L. A. Lugiato and R. Lefever, *Phys. Rev. Lett.* **58**, 2209 (1987).
- [22] Y. K. Chembo and C. R. Menyuk, *Phys. Rev. A* **87**, 053852 (2013).
- [23] S. Coen, H. G. Randle, T. Sylvestre, and M. Erkintalo, *Opt. Lett.* **38**, 37 (2013).
- [24] C. R. Lourés, D. Faccio, and F. Biancalana, *Phys. Rev. Lett.* **115**, 193904 (2015).
- [25] J. Pfeifle, A. Coillet, R. Henriot, K. Saleh, P. Schindler, C. Weimann, W. Freude, I. V. Balakireva, L. Larger, C. Koos, and Y. K. Chembo, *Phys. Rev. Lett.* **114**, 093902 (2015).
- [26] T. Hansson and S. Wabnitz, *Nanophotonics* **5**, 231 (2016).
- [27] T. J. Kippenberg, R. Holzwarth, and S. A. Diddams, *Science* **332**, 555 (2011).
- [28] S. T. Cundiff, J. Ye, and J. L. Hall, *Review of Scientific Instruments* **72**, 3749 (2001), https://pubs.aip.org/aip/rsi/article-pdf/72/10/3749/19059716/3749_1_online.pdf.
- [29] V. Torres-Company and A. M. Weiner, *Laser & Photonics Reviews* **8**, 368 (2014).
- [30] E. Temprana, E. Myslivets, B.-P. Kuo, L. Liu, V. Ataie, N. Alic, and S. Radic, *Science* **348**, 1445 (2015).
- [31] D. Martín and M. Hoyuelos, *Physica D: Nonlinear Phenomena* **259**, 37 (2013).
- [32] G. D'Aguzzo and C. R. Menyuk, *The European Physical Journal D* **71**, 1 (2017).
- [33] C. Milián, Y. V. Kartashov, D. V. Skryabin, and L. Torner, *Opt. Lett.* **43**, 979 (2018).
- [34] K. Panajotov, M. Tlidi, Y. Song, and H. Zhang, *Chaos, Solitons & Fractals* **163**, 112532 (2022).
- [35] Q.-H. Cao, K.-L. Geng, B.-W. Zhu, Y.-Y. Wang, and C.-Q. Dai, *Chaos, Solitons & Fractals* **166**, 112895 (2023).
- [36] M. Saha, S. Roy, and S. K. Varshney, *Phys. Rev. A* **101**, 033826 (2020).
- [37] B. Kostet, Y. Soupart, K. Panajotov, and M. Tlidi, *Phys. Rev. A* **104**, 053530 (2021).
- [38] A. Sahoo and S. Roy, *Phys. Rev. A* **100**, 053814 (2019).
- [39] S. Fujii, A. Hori, T. Kato, R. Suzuki, Y. Okabe, W. Yoshiki, A.-C. Jinnai, and T. Tanabe, *Opt. Express* **25**, 28969 (2017).
- [40] W. B. Cardoso, L. Salasnich, and B. A. Malomed, *Sci. Rep.* **7**, 16876 (2017).
- [41] W. B. Cardoso, L. Salasnich, and B. A. Malomed, *Eur. Phys. J. D* **71**, 112 (2017).
- [42] S. Kumar, W. B. Cardoso, and B. A. Malomed, *Symmetry*

- [16](#), [10.3390/sym16040470](#) (2024).
- [43] M. C. P. dos Santos, S. Kumar, W. B. Cardoso, and B. A. Malomed, *Phys. Rev. E* **111**, 014207 (2025).
- [44] N. Hacker and B. A. Malomed, *Symmetry* **13**, [10.3390/sym13030372](#) (2021).
- [45] M. C. P. dos Santos and W. B. Cardoso, *Phys. Rev. E* **103**, 052210 (2021).
- [46] M. C. P. dos Santos and W. B. Cardoso, *Nonlinear Dyn.* **111**, 3653 (2023).
- [47] M. C. P. dos Santos, D. Bazeia, A. T. Avelar, and W. B. Cardoso, *Nonlinear Dyn.* **113**, 1539 (2025).
- [48] J. Yang, *Nonlinear Waves in Integrable and Nonintegrable Systems* (Society for Industrial and Applied Mathematics, 2010).